

# CD<sup>2</sup>: Fine-grained 3D Mesh Reconstruction with Twice Chamfer Distance

RONGFEI ZENG\*, MAI SU\*, RUIYUN YU, and XINGWEI WANG<sup>†</sup>, Northeastern University, China

Monocular 3D reconstruction is to reconstruct the shape of object and its other information from a single RGB image. In 3D reconstruction, polygon mesh, with detailed surface information and low computational cost, is the most prevalent expression form obtained from deep learning models. However, the state-of-the-art schemes fail to directly generate well-structured meshes, and most of meshes have two severe problems Vertices Clustering (VC) and Illegal Twist (IT). By diving into the mesh deformation process, we pinpoint that the inappropriate usage of Chamfer Distance (CD) loss is the root causes of VC and IT problems in the training of deep learning model. In this paper, we initially demonstrate these two problems induced by CD loss with visual examples and quantitative analyses. Then, we propose a fine-grained reconstruction method CD<sup>2</sup> by employing Chamfer distance twice to perform a plausible and adaptive deformation. Extensive experiments on two 3D datasets and comparisons with five latest schemes demonstrate that our CD<sup>2</sup> directly generates well-structured meshes and outperforms others by alleviating VC and IT problems.

CCS Concepts: • **Computing methodologies** → **Reconstruction**; Shape representations.

Additional Key Words and Phrases: 3D reconstruction, machine learning, chamfer distance, mesh deformation

## ACM Reference Format:

Rongfei Zeng, Mai Su, Ruiyun Yu, and Xingwei Wang. 2022. CD<sup>2</sup>: Fine-grained 3D Mesh Reconstruction with Twice Chamfer Distance. *J. ACM* 37, 4, Article 111 (August 2022), 21 pages. <https://doi.org/XXXXXXX.XXXXXX>

## 1 INTRODUCTION

Monocular 3D mesh reconstruction, boosted by deep learning, is a fundamental and fascinating topic in the community of computer vision. It aims to generate detailed 3D information of the object's surface, orientation, etc. in mesh format from a single 2D image [19]. The prevalent data format of mesh, which consists of hundreds of vertexes and faces, has plenty of features and advantages. For instance, mesh can efficiently and accurately capture the details of 3D objects' surfaces and describe almost every shape in the world, such as cars, boats, and airplanes in ShapeNet dataset [6]. Meanwhile, the quality of mesh has been drastically improved by the promising deep learning technique and large-scale datasets in recent years [6, 31]. All these benefits empower explicit 3D mesh reconstruction with deep learning [43] to have widespread applications in 3D printing, automatic drive, virtual/augmented reality, medical diagnosis, and online shopping [20].

\*Both authors contributed equally to this paper.

<sup>†</sup>Corresponding author

Authors' address: Rongfei Zeng, [zengrf@swc.neu.edu.cn](mailto:zengrf@swc.neu.edu.cn); Mai Su, [sumai1998@foxmail.com](mailto:sumai1998@foxmail.com); Ruiyun Yu, [yury@mail.neu.edu.cn](mailto:yury@mail.neu.edu.cn); Xingwei Wang, [wangxw@mail.neu.edu.cn](mailto:wangxw@mail.neu.edu.cn), Northeastern University, No. 11, Wenhua Street, Heping District, Shenyang, Liaoning, China, 110819.

Permission to make digital or hard copies of all or part of this work for personal or classroom use is granted without fee provided that copies are not made or distributed for profit or commercial advantage and that copies bear this notice and the full citation on the first page. Copyrights for components of this work owned by others than ACM must be honored. Abstracting with credit is permitted. To copy otherwise, or republish, to post on servers or to redistribute to lists, requires prior specific permission and/or a fee. Request permissions from [permissions@acm.org](mailto:permissions@acm.org).

© 2022 Association for Computing Machinery.

0004-5411/2022/8-ART111 \$15.00

<https://doi.org/XXXXXXX.XXXXXX>

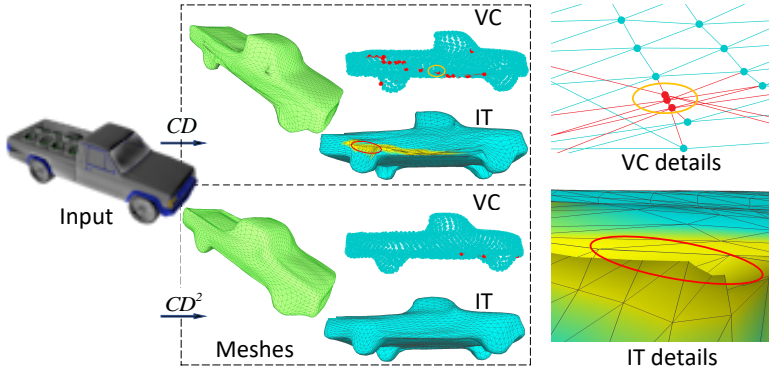


Fig. 1. IT and VC problems in 3D mesh reconstructions and our improvement with  $CD^2$ .

In the deep-learning-enabled mesh reconstruction, Chamfer Distance (CD) [2] is a universally-adopted and paramount component used as the loss function of deep learning model as well as the metric to measure quality of generated 3D mesh model. CD calculates the average of pairwise nearest neighbour distance between the synthetic mesh and the ground truth object. CD is preferable for explicit mesh reconstruction due to its efficient computation and flexible applicability with different volumes of points. The vast majority of impressive works such as Atlasnet [12], TMN [24], and Pixel2Mesh [37] employ CD as a loss function or part of loss function for model training and achieve acceptable model performance.

However, CD has some intrinsic deficiencies and some previous studies have been published to identify them. For instance, Li et al. show that CD may suffer from the local optimum problem in its nearest neighbor search [14]. Wu et al. reiterate that CD is insensitive to point density distribution and is prone to be impacted by outliers [39]. Jin et al. demonstrate that CD may not be faithful visually and structurally [13]. Achlioptas et al. find that CD is inclined to generate overcrowded points in some visible areas of object in the input image [1]. Wagner et al. empirically prove that directly optimizing CD will ignore details of some structure [34]. Meanwhile, researchers also propose some variant CDs, such as a structured CD [14], a sharper version of CD [16], an adaptive CD [35], a probabilistic CD [15], an augmented CD [7], a density-aware CD [39], etc., and attempt to fix the above defects caused by CD loss.

Even worse, we find that CD loss still suffers from IT and VC problems, which have not been discovered by previous studies. As shown in Fig. 1, IT problem refers to the situation where some faces locally and irrationally intersect with others or interpose into the inner regions, while VC problem describes the scenario where many vertices cluster around a single ground truth point. Empirically, both IT and VC problems are attributed to CD loss function which offers incorrect deformation directions in the brute-force nearest neighbour search. The consequence of these two problems is performance degradation caused by wasting limited vertices in some invisible and overcrowded regions and distorting the mesh into an unusable structure. Furthermore, these severe problems might malfunction the downstream applications of 3D reconstruction, such as 3D printing, rendering, etc. In a nutshell, IT and VC problems introduced by CD loss should be considered seriously in the explicit mesh reconstruction.

In this paper, we take a deep dive into the IT and VC problems and endeavor to improve the quality of reconstructed mesh with the idea of twice CD calculation in deep learning method. Staring with the identification of IT and VC problems in both visual and quantitative ways, we find that some vertices of generated mesh move in incorrect directions or at a much aggressive

Table 1. Notations frequently used in this paper.

Notations	Explanations
$S_1$	The ground truth point set of target 3D object
$S_2$	The vertex set of synthetic mesh
$V_i$	The $i$ -th vertex in the mesh set $S_2$
$P_j$	The $j$ -th point in the ground truth point set $S_1$
$\phi(V_i)$	$V_i$ 's nearest point in $S_1$
$\psi(P_j)$	$P_j$ 's nearest vertex in $S_2$
$\mathbb{P}_{V_i}$	Points in $S_1$ whose nearest vertex in $S_2$ is $V_i$
$\mathbb{V}_{P_j}$	Vertices in $S_2$ whose nearest point in $S_1$ is $P_j$

speed. Following these observations, we provide our proposal CD<sup>2</sup> to perform a fine-grained mesh generation process. The proposed CD<sup>2</sup> calculates the CD metric twice and excludes some excessively-moving vertices from further deformation with three criteria, which makes vertices deform with a comparable speed in correct directions. Comparing with five impressive works on two datasets ShapeNet and Pix3D, we demonstrate our scheme CD<sup>2</sup> can effectively and efficiently mitigate IT and VC problems and yield a well-structured 3D mesh model.

The contributions of this paper are threefold:

- To the best of our knowledge, we are the first to identify IT and VC problems caused by CD loss in deep learning model of 3D reconstruction and provide both visual examples and quantitative analyses of these two problems. 28% vertices have VC problems on average ( $\rho = 0.5$ ) in famous Atlasnet [12], and 28.1% faces have IT problems in Total3D [21].
- We propose an innovative approach CD<sup>2</sup> with twice CD calculation to mitigate IT and VC problems by moving vertices in a moderate speed and rational directions. Our proposal CD<sup>2</sup> achieves a fine-grained deformation process.
- Visual demonstrations show our CD<sup>2</sup> generates more plausible and well-structured meshes than other five baseline schemes. Meanwhile, quantitative evaluation results reveal that our CD<sup>2</sup> outperforms other baselines in terms of several metrics. Some mesh quality metrics, provided by our work which consider the distance or mapping relation, achieve the faithful and appropriate measuring capability.

The remainder of this paper is organized as follows. In Section 2, we identify the IT and VC problems and formalize these problems. Section 3 presents our proposed method CD<sup>2</sup>. Extensive experiment results are presented in Section 4, followed by related work in Section 5. Section 6 concludes the entire paper.

## 2 PROBLEM STATEMENT AND ANALYSIS

### 2.1 Chamfer Distance

Chamfer distance, proposed by Barrow et al. in [2], is a universally-adopted metric to measure the pair-wise average nearest distance between two point sets. In deep learning model of 3D mesh reconstruction, CD is chosen as the loss function in the optimization process and the evaluation metric of 3D mesh quality. Mathematically, CD is defined as

$$d_{CD}(S_1, S_2) = \frac{1}{|S_1|} \sum_{x \in S_1} \min_{y \in S_2} \|x - y\|_2 + \frac{1}{|S_2|} \sum_{y \in S_2} \min_{x \in S_1} \|x - y\|_2,$$

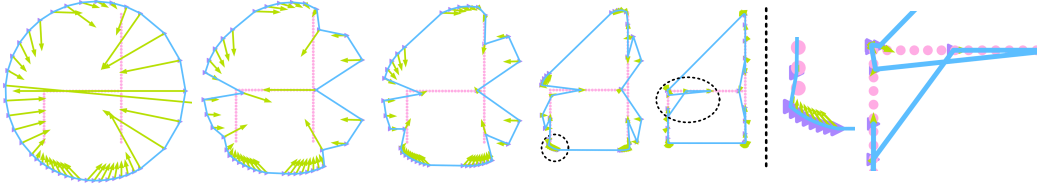


Fig. 2. A toy 2D chair deformation example and the details of VC and IT problems. We use pink dot to denote ground truth points, purple triangle to denote mesh vertices, blue line to denote edges between vertices, and cyan arrow to denote gradients of vertices. The deformation gradients are computed with CD loss. We also zoom in on the IT and VC problems in the 6th subfigure.

where  $S_1 \subseteq \mathbb{R}^3$  is the ground truth point set and  $S_2 \subseteq \mathbb{R}^3$  is the reconstructed mesh vertex set<sup>1</sup>. The calculation of CD is composed of two components  $d_{CD1}$  and  $d_{CD2}$ . The term  $d_{CD1}$  considers the average distance from a point in the ground truth set  $S_1$  to its nearest vertices in  $S_2$ , while the second term  $d_{CD2}$  evaluates the average distance from a vertex in mesh  $S_2$  to its nearest point in  $S_1$ .

In most scenarios, we have  $|S_1| \gg |S_2|$ . For instance, each ground truth 3D object consists of 10,000 points in Pix3D dataset [21] and 30,000 points in ShapeNet [6], while the sphere template for deformation only use 2,562 vertices in both Total3D [21] and Atlanset [12] due to limitations of computing resources. In such scenarios, we should not waste limited vertices inside meshes, and they are required to be used efficiently to model the surface of a target object. For simplicity, we list some commonly-used notations in Table 1.

## 2.2 A Toy Example of Mesh Deformation Process with CD Loss

In this subsection, we present a toy example to demonstrate the mesh deformation process with CD loss in Fig. 2. In this example, we use 81 pink dots (ground truth set  $S_1$ ) to model a wooden chair and 40 purple triangles connected by blue edges to represent a mesh template set  $S_2$ . We first calculate CD between these two sets and use the API `torch.Tensor.backward()` in PyTorch to obtain the gradient of each vertex and shown the deformation gradient by cyan line with arrow (deformation gradient has the equal magnitude but opposite direction to mathematical gradient). During each deformation, we follow each deformation gradient to move the corresponding vertex. This deformation process iterates until the CD loss is minimized or the number of iteration times exceed the predefined threshold. When the deformation process is finished, the generated mesh almost models the target chair. Some deformation snapshots are given in Fig. 2.

We have two observations from this deformation process in Fig. 2. (1) Many vertices in  $S_2$  crowd in small and specific regions like the end of legs and chair back in this example. We explicitly present these over-crowded vertices with dotted circles and name this phenomenon as Vertices Clustering (VC). Actually, there is no need to waste the excessive number of vertices to model chair back and the end of legs, and some vertices are better to approach to other important details like the cushion surface of chair. (2) In our toy example, there exist some unnecessary and intersected lines shown in the dotted circle of the 5th subfigure. We zoom in on this part in the next subfigure. Similarly, some vertices rush into the interior of chair cushion and generate the unexpected twist of faces in 3D deformation process, which can be found in Section 4. No vertex is needed to model the interior of a chair, and it is the best practice to use enough vertices to describe the surface of cushion. The aggressive deformation of these vertices causes the generated mesh to have intersected and twisted faces and not properly align with the target object. We call this phenomenon Illogical Twist

<sup>1</sup>We use the term vertex to denote point in the reconstructed mesh for readability.



(IT). Both VC and IT are induced by CD loss which only pursues the point-level similarity in the brute-force nearest neighbour search, ignoring the edge relations of the mesh and the overall shape of the target object. In the next subsection, we present the definitions of IT and VC, and try to analyze the underlying cause of these two problems.

### 2.3 The Definitions of VC and IT Problems

**Vertices Clustering.** VC describes the scenario where multiple mesh vertices crowd or overlap with each other in a small region as shown in Fig. 1. The formal definition of VC is given as follows:

**DEFINITION 1.** *Vertices Clustering: Let  $\bar{d}(S_1)$  be the average nearest neighbor distance between points in  $S_1$ , and define the distance threshold between two vertices in  $S_2$  as  $\sigma_{VC} = \rho \bar{d}(S_1)$ , where the coefficient  $\rho$  is a hyper-parameter. Then, we have two criteria to evaluate VC problem: (1) the size of VC vertex set  $S_{VC} \subseteq S_2$ , where each vertex  $V_i \in S_{VC}$  has the nearest neighbor  $V_j$  in  $S_2$  and this nearest neighbor distance is smaller than  $\sigma_{VC}$ , i.e.,  $d(V_i, V_j) < \sigma_{VC}$ . In other words, we can use  $N_{VC} = |S_{VC}|$  to evaluate the VC problem; and (2) the number of vertices  $V_i$  in  $S_{VC}$  which have identical nearest ground truth points in  $S_1$  with other  $V_j \in S_{VC}$ , i.e.,  $(d(V_i, V_j) < \sigma_{VC}) \& (\phi(V_i) = \phi(V_j))$ .*

We have some takeaways from this definition. Initially, we argue that VC endeavours to find vertices which are extremely close to each other during deformation. Since one goal of mesh deformation is to evenly distribute vertices over the surface of the target object, we can coordinate the deformation process with the VC constraint to alleviate the overcrowding problem and efficiently distribute vertices in a fine-grained manner. In addition, these two criteria of VC can be used as the quality evaluation metric of synthetic mesh as well. Finally, we can easily find that the second criterion is much stricter than the first one.

Based on our formal definition, VC problem universally exists in previous CD-based deformation schemes. In Table 4, we present the results of VC problem for Atlasnet [12]. We can find that the classes of rifle, lamp, and airplane are prone to have VC problems. For a rifle, there are 367 VC vertices of the first type (i.e.,  $N_{VC} = 367$ ) among 2562 total vertices and 314 VC vertices of the second type (i.e.,  $N_{VC'} = 314$ ), when  $\rho = 0.25$ . The average percentage of first-type VC vertices ( $N_{VC}/|S_2|$ ) and the average percentage of second-type VC vertices ( $N_{VC'}/|S_2|$ ) are separately 14.3% and 12.3% for the class of rifle. Even worse, when  $\rho = 0.5$ , the average VC percentages separately reach 28.1% and 20.9% for all the categories. Similar results can be found in other classes and models.

**Illogical Twist.** IT refers to the situation where some parts of the mesh intersect with itself or rush into the inner region as shown in Fig. 1. The IT problem can be formally defined as follows:

**DEFINITION 2.** *Illegal Twist: For two faces  $f_i$  and  $f_j$ , let  $v(f_i, f_j)$  denote the number of shared vertices between these two faces. If  $v(f_i, f_j) = 0$ , we use the algorithm in [41] to determine whether  $f_i$  intersects with  $f_j$  or not and then construct a IT face set  $S_{IT}$  with this algorithm. Then, we have two criteria to evaluate IT problem: (1) the size of IT face set,  $F_{IT} = |S_{IT}|$ ; and (2)  $V_{IT}$ , the number of vertices which belong to the faces in  $S_{IT}$ .*

The IT phenomenon also occurs universally in the reconstructed mesh of Atlasnet in Fig. 5 and Total3D in Fig. 6. Fig. 5 shows the IT problem with yellow marked faces, while Fig. 6 presents this problem with wireframes from different views. Besides the visual results, we also use two types of IT metrics to evaluate the results of Atlasnet in Table 4. It can be found that the reconstructed meshes of table, rifle, chair, and bench have severe IT problems. For the class of table, there exist 809.5 IT faces of first-type IT metrics on average and 677.8 vertices of the second-type of IT metrics. The percentages are separately 15.8% and 26.5%. These results seem to be astonishing, and the output yields an unacceptable and valueless mesh model which is not suitable for applications in downstream tasks.

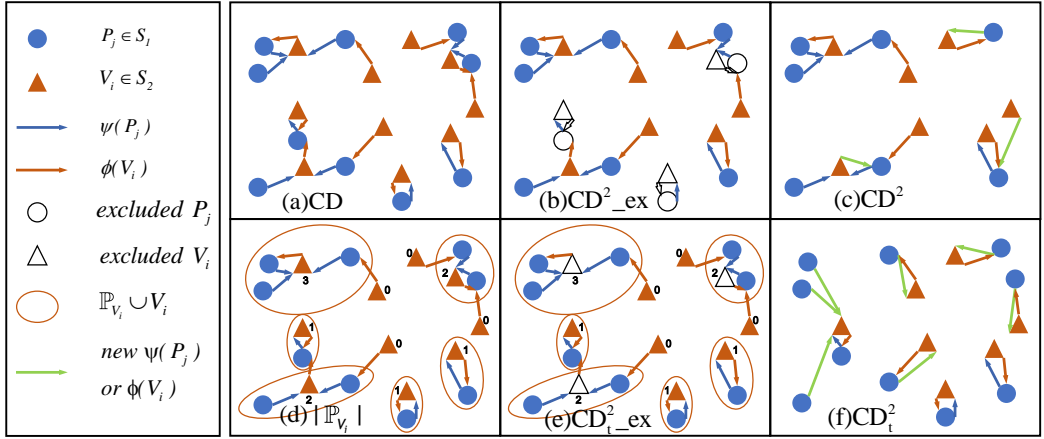


Fig. 3. The deformation demonstrations of CD, the distance-oriented  $CD^2$ , and the mapping-oriented  $CD_t^2$ . (a) The nearest neighbour relation of CD; (b) vertices exclusion in  $CD^2$ ; (c) the new vertex-point mapping relation of  $CD^2$ ; (d)  $|P_{V_i}|$ ; (e) vertices exclusion in  $CD_t^2$ ; and (f) the new vertex-point mapping relation of  $CD_t^2$  ( $poi_i=1.5$ ). We show the legend in the left column.

Why do the VC and IT problems occur in the deformation process? Typically, ground truth points are uniformly distributed across the 3D object's surface in the dataset, but 2D objects in the image are presented in a fixed view. Learning from images with partially visible objects and unbalanced confidence levels leads to unreasonable gradient directions and a huge deformation velocity gap. In other words, visible parts of objects in the image have a larger deformation gradient than those invisible parts. Even worse, some excessively-deformed mesh vertices still have a large deformation velocity after arriving at the target positions but cannot stop moving in the brute-force nearest neighbour search, as shown in Fig. 2. This over-deformation ultimately results in the intersection and twist of mesh faces and overcrowded vertices in a small region. From the above illustration, we can identify VC and IT vertices and then orchestrate them at an appropriate velocity to prevent the output mesh from VC and IT problems.

### 3 OUR FINE-GRAINED MESH RECONSTRUCTION SCHEME $CD^2$

In this section, we provide two fine-grained 3D mesh reconstruction schemes  $CD^2$  both of which compute CD metrics twice in one iteration of mesh deformation. In other words, each deformation iteration is divided into two sub-steps. The first step involves vertices exclusion by calculating the CD loss, and we compute the CD metric twice for residual vertices in the second step, instead of considering all the vertices equally and moving them aggressively. According to different considerations for vertices exclusion in the first step, our proposal  $CD^2$  contains two versions, i.e., the distance-oriented  $CD^2$  and the mapping-oriented  $CD^2$ .

#### 3.1 The Distance-oriented $CD^2$

We first present our intuitive and efficient scheme distance-oriented  $CD^2$  which utilizes the distance information to exclude those aggressive vertices. In the first step of distance-oriented  $CD^2$ , we compute CD metrics for all the vertices, identify those excessively-deformed vertices, and exclude them from the next deformation according to distance information. In the second step, our scheme computes another CD metric for residual vertices and moves them according to the new gradients.

**Algorithm 1:** The Distance-oriented CD<sup>2</sup>**Input:**  $S_1, S_2, p_d, d_T$ **Output:**  $d_{CD^2}(S_1, S_2)$  $Dist_1, Dist_2, index_1, index_2 = d_{CD}(S_1, S_2)$  $|S_{2d}| = \max(p_d \times |S_2|, |Dist_2| < d_T)$ **for**  $i = 1$  **to**  $|S_2|$  **do**    **if**  $Dist_2[i]$  **is top**  $|S_{2d}|$  **smallest** **then**        Append  $S_2[i]$  to  $S_{2d}$         Append  $S_1[Index_2[i]]$  to  $S_{1d}$     **end****end** $S'_1 = S_1 - S_{1d}$  $S'_2 = S_2 - S_{2d}$  $Dist'_1, Dist'_2 \leftarrow d_{CD}(S'_1, S'_2)$  $d_{CD^2}(S_1, S_2) = \text{Mean}(Dist'_1) + \text{Mean}(Dist'_2)$ 

Before introducing the vertex exclusion method in the first step, we present four critical data structures used in the following paper as follows:

- $Dist_1$  and  $Index_1$ . In the nearest distance list  $Dist_1$ , the element  $Dist_1[i]$  is the distance from point  $P_i \in S_1$  to its corresponding nearest vertex  $V_j \in S_2$ . We also put the index of this nearest vertex  $j$  into the list  $Index_1$ , i.e.,  $Index_1[i] = j$ .
- $Dist_2$  and  $Index_2$ . In the nearest distance list  $Dist_2$ , the element  $Dist_2[i]$  is the distance from vertex  $V_i \in S_2$  to its corresponding nearest point  $P_j \in S_1$ . We also put the index of this nearest point into the list  $Index_2$ , i.e.,  $Index_2[i] = j$ .

In the following, we provide a simple and useful method to identify those aggressive vertices which are extremely close to the ground truth point set and then exclude them from further deformation. This method conforms to the empirical insight that we should move all the vertices at a comparable velocity to alleviate the VC and IT problems. In detail, we construct an exclusion vertices set  $S_{2d}$  and its size is determined by two factors, i.e.,  $|S_{2d}| = \max\{[p_d \times |S_2|], n_t\}$ , where the threshold  $p_d \in (0, 1)$  is the percentage of vertices excluded from the next CD computation and  $n_t \in (0, |S_z|)$  is the number of vertices whose nearest point distance is smaller than the threshold  $d_T$ . With our previous data structures  $Dist_2$  and  $Index_2$ , we can easily find those vertices with a certain nearest distance. Then, we can construct a vertex set  $S'_2 = S_2 - S_{2d}$ . Meanwhile, we can obtain the set  $S_{1d}$  by mapping the  $S_{2d}$  through  $Index_2$  and get the corresponding new ground truth point set  $S'_1$  for further CD computation. In the second step, we compute another CD loss for these new sets  $S'_1$  and  $S'_2$  and only move vertices in  $S'_2$  to the ground truth points. The detailed algorithm is presented in Algorithm 1.

In Algorithm 1, both mesh vertices and ground truth points are changed according to their distance relationships in the second step of each deformation iteration, which makes our distance-oriented CD<sup>2</sup> more adaptive than before. In addition, the selection of vertex for deformation enables the generated mesh to approach to the target 3D object in a synchronization manner, which further relieves VC and IT problems. Finally, we should note that the computational cost is not increased too much, although we compute CD twice. Both the number of vertices and points are reduced in the second step of CD<sup>2</sup>. Our distance-oriented CD<sup>2</sup> still dominates EMD in terms of computational cost, which will be further analyzed in Section 4.5.

---

**Algorithm 2:** The Mapping-oriented  $CD^2$ 


---

**Input:**  $S_1, S_2, pvi_t, pvi_p$ **Output:**  $d_{CD^2}(S_1, S_2)$ **Function**  $Exclude(Index_1, Index_2, pvi_t, pvi_p, S_2)$ :

```

for  $j = 1$  to  $|Index_1|$  do
     $Pv[Index_1[j]] = Pv[Index_1[j]] + 1$ 
end
if  $apply\ CD_t^2$  then
    for  $i = 1$  to  $|S_2|$  do
        if  $Pv[i] > pvi_t$  then
            Append  $S_2[i]$  to  $S_{2d}$ 
        end
    end
end
if  $apply\ CD_p^2$  then
    for  $i = 1$  to  $|S_2|$  do
        if  $Pv[i]$  is top  $pvi_p$  largest then
            Append  $S_2[i]$  to  $S_{2d}$ 
        end
    end
end
 $S'_2 = S_2 - S_{2d}$ 
return  $S'_2$ 

```

 $Dist_1, Dist_2, index_1, index_2 = d_{CD}(S_1, S_2)$  $S'_2 = Exclude(Index_1, Index_2, pvi_t, pvi_p, S_2)$  $S'_1 = Exclude(Index_2, Index_1, pvi_t, pvi_p, S_1)$  $Dist'_1, Dist'_2 = d_{CD}(S'_1, S'_2)$  $d_{CD^2}(S_1, S_2) = Mean(Dist'_1) + Mean(Dist'_2)$ 


---

### 3.2 The Mapping-oriented $CD^2$

Besides the distance information between the vertex set  $S_2$  and ground truth point set  $S_1$ , additional information on mapping relation can also be utilized to orchestrate the deformation process. In this subsection, we present another fine-grained  $CD^2$  based on the point-vertex mapping information. Initially, we define a new data structure  $\mathbb{P}_{V_i}$  to denote the set of points that consider  $V_i \in S_2$  as their nearest vertex, i.e.,  $\psi(P_l) = V_i, \forall P_l \in \mathbb{P}_{V_i}$ . The larger size of  $\mathbb{P}_{V_i}$  indicates that vertex  $V_i$  is extremely close to the target object, which might not be appropriate for further deformation. From the definition of  $\mathbb{P}_{V_i}$ , we can find that this mapping relation contains more information and somehow includes the distance information. This benefit improves the mesh reconstruction performance, which will be extensively studied in Section 4. Moreover, the vertex-point mapping information  $|\mathbb{P}_{V_i}|$  can not only guide the training but also be applied to measure the quality of mesh as shown in Table 2

In the following, we use  $|\mathbb{P}_{V_i}|$  to exclude some vertices and guide the model learning. In this paper, we provide two specific exclusion methods with vertex-point mapping relation information. One approach  $CD_t^2$  eliminates vertices whose  $|\mathbb{P}_{V_i}|$  is larger than a predefined threshold  $pvi_t$ , while another approach  $CD_p^2$  just eliminates a certain percentage  $pvi_p$  of vertices with largest  $|\mathbb{P}_{V_i}|$  value. Similarly, we can also delete points according to their  $|\mathbb{V}_{P_j}|$  in  $S_1$ . Then, we remove these

vertices from  $S_2$  and move residual vertices to the ground truth points in the second CD calculation. The details of our mapping-oriented methods are presented in Algorithm 2. Finally, we show the deformation process of the traditional CD, our proposal CD<sup>2</sup>, and CD<sub>*t*</sub><sup>2</sup> ( $pvi_t=1.5$ ) in Fig. 3.

#### 4 EXPERIMENTS AND EVALUATIONS

In this section, we perform extensive experiments to demonstrate the improvement of our proposals. We compare our proposed methods CD<sup>2</sup>, CD<sub>*t*</sub><sup>2</sup>, and CD<sub>*p*</sub><sup>2</sup> with three representative baselines Atlasnet [12] on ShapeNet dataset [6], 3DAF [44] on ShapeNet, and Total3D [21] on Pix3D dataset [31]. All these works deform a template directly with CD loss. Besides these CD-related works, we also compare two recent Signed Distance Fields (SDF) works Im3d [45] and Tars3d [50] in terms of the mesh quality. Our comparison results are shown by visual demonstration and quantitative analyses with a variety of metrics including our proposed metrics  $N_{VC}$ ,  $N_{VC'}$ ,  $F_{IT}$ ,  $P_{IT}$  and DPVI. Finally, the time consumption of our various metrics is compared.

Table 2. Statistical results of DPVI on Atlasnet. We present the number of test samples in each  $|\mathbb{P}_{V_i}|$  category. A large value is preferred for  $|\mathbb{P}_{V_i}| = 1$ , while we prefer values close to OPTA for  $|\mathbb{P}_{V_i}| = 2$ . Otherwise, the smaller is better.

$ \mathbb{P}_{V_i} $	0	1	2	3-10	11-20	21-30	31-40	41-50	51-max
At <sub>CD</sub>	1154.0	765.2	383.3	258.1	1.369	0.104	0.019	0.006	0.005
CD <sup>2</sup>	1186.4	740.6	368.8	264.0	2.114	0.158	0.034	0.009	0.005
CD <sub><i>p</i></sub> <sup>2</sup>	1138.5	<b>774.1</b>	392.5	<b>255.8</b>	0.984	<b>0.065</b>	<b>0.012</b>	0.004	<b>0.003</b>
CD <sub><i>t</i></sub> <sup>2</sup>	<b>1137.8</b>	773.9	<b>393</b>	256.3	<b>0.929</b>	0.066	0.0124	<b>0.003</b>	<b>0.003</b>
OPTA	1122.8	780.8	397.3	261	0.025	0	0	0	0.000
Im3d	1329.5	601.1	327.1	299.7	3.62	0.67	0.202	0.084	0.08
Tars3d	1648.6	329.7	222.7	348.5	11.4	0.876	0.18	0.062	0.075

##### 4.1 Comparisons with Atlasnet on ShapeNet

We first compare the performance of our CD<sup>2</sup>, CD<sub>*p*</sub><sup>2</sup>, and CD<sub>*t*</sub><sup>2</sup> with the famous scheme Atlasnet [12] on ShapeNet [6]. ShapeNet dataset contains 35K manually-created 3D CAD samples, each of which involves a polygon mesh and several rendered pictures from different views. The 13 categories of ShapeNet include airplane, bench, cabinet, car, etc. Atlasnet is an impressive 3D mesh reconstruction method which is composed of 3 modules, i.e., the autoencoder trained decoder, the subsequent ResNet encoder, and the final single-view reconstruction module. Since we find that the first module of Atlasnet generates meshes with appropriate topology structures better than the other two modules, we only use the output of the first module as baseline in this paper. In addition, multiple patches in Atlasnet are prone to generate VC and IT problems, so we use 1 patch of sphere for Atlasnet in our experiments.

We use the pretrained model provided by the Atlasnet [12] as At<sub>CD</sub>, and implement our methods in Atlasnet with the following settings. For the CD<sup>2</sup> method, we set  $p_d = 0.3$ ,  $d_T = 10^{-7}$ . For our CD<sub>*t*</sub><sup>2</sup>, we exclude both the vertices and points with  $pvi_t = 4$ . For the CD<sub>*p*</sub><sup>2</sup>, we set  $pvi_p = 0.08$  for the vertex set  $S_2$  and exclude  $S_1$  at the ratio of 0.01. All our learning rates are  $10^{-4}$ .

We use Meshlab [8] to present our visual results in Fig. 4 and Fig. 5. From these results, we can easily find that our proposed schemes, especially the mapping-oriented CD<sub>*p*</sub><sup>2</sup> and CD<sub>*t*</sub><sup>2</sup>, generate better mesh models than the baseline At<sub>CD</sub>. For simple objects such as car and sofa, our CD<sub>*t*</sub><sup>2</sup>

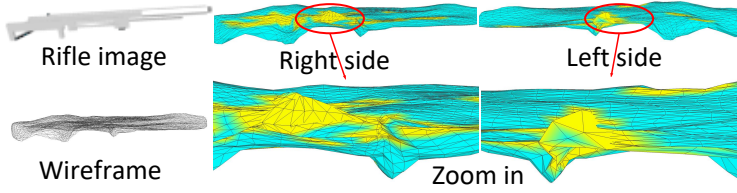


Fig. 4. The mesh of rifle with  $At_{CD}$ .

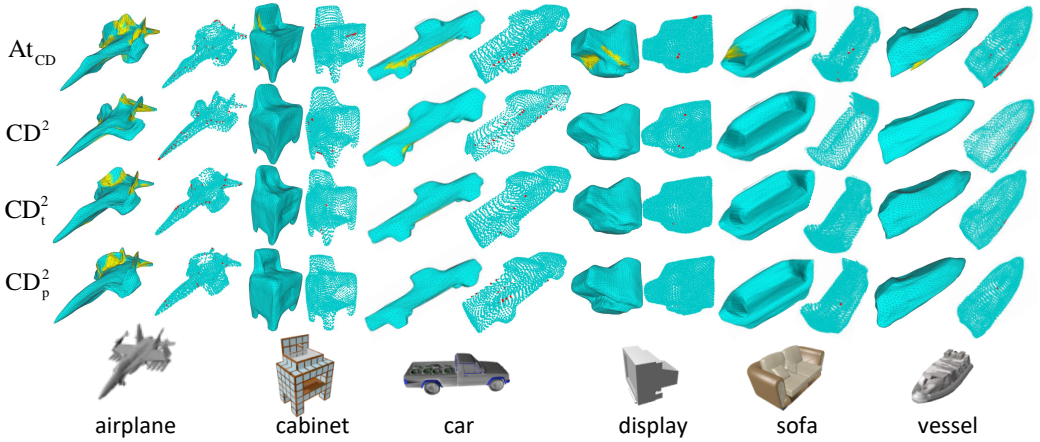


Fig. 5. Meshes on ShapeNet. We show the outputs of  $At_{CD}$ ,  $CD^2$ ,  $CD_t^2$ , and  $CD_p^2$  from the top row from the bottom one. IT faces are shown in yellow, while VC vertices are presented in red.

almost eliminates IT and VC problems. For more complicated objects like airplane, VC and IT problems are alleviated by our schemes, while they are quite severe in the baseline  $At_{CD}$ . Finally, some IT problems still appear in some objects like rifles, the performance improvement for these categories is left for future work, although our work has already improved their performance.

The quantitative results with the CD and EMD metrics are shown in Table 3. Note that the CD metric is amplified by  $10^4$  for easy comparisons in Table 3. The comparison results for VC and IT problems are shown in Table 4. To further demonstrate the performance improvement for VC and IT problems, we present the statistical information of the vertex-point mapping relation. We define DPVI as the number of vertices who has the same value of  $|\mathbb{P}_{V_i}|$ . In other words, it shows the information how many ground truth points are described by a single mesh vertex. Obviously, large  $|\mathbb{P}_{V_i}|$  is not desired by mesh reconstruction tasks. The statistical results for DPVI are presented in Table 2. Our results except Table 4 are computed over the entire test set. In Table 4, we average 32 samples for VC and 10 samples for IT due to the experimental duration consideration. We find that these results can be generalizable to the entire test set. We also present the Optimum Performance Theoretically Attainable (OPTA) for CD, EMD, and DPVI by randomly selecting 2562 points from 30K ground truth points twice and computing these metrics. Finally, we bold all the best results in the above tables.

Our proposed schemes  $CD_p^2$  and  $CD_t^2$  outperform others for all the metrics except CD value. Compared with  $At_{CD}$ , our  $CD_t^2$  lowers EMD value by 37.9% on average. In addition, VC vertices and IT faces are separately reduced by 31.4% and 24.0%. Our results also demonstrate that point-vertex mapping relation is more suitable for 3D mesh reconstruction than the distance relation, which is

Table 3. CD and EMD on Atlasnet. Smaller value is preferred.

Method	Metric	airplane	bench	cabinet	car	chair	display	lamp	speaker	rifle	sofa	table	telephone	vessel	all
At <sub>CD</sub>	CD	<b>8.1</b>	<b>10.87</b>	<b>13.45</b>	14.7	<b>14.4</b>	<b>13.5</b>	<b>21.9</b>	<b>20.15</b>	6.02	13.6	<b>13.9</b>	10.4	<b>12.2</b>	<b>13.3</b>
	EMD	52.1	46.3	46.9	52.1	59.2	57.2	166.0	56.1	63.9	39.5	67.4	53.9	61.9	63.3
CD <sup>2</sup>	CD	9.6	12.4	14.1	16.5	16.2	14.6	25.6	21.5	7.1	14.4	15.9	10.8	14.2	14.8
	EMD	108.6	176.9	165.2	93.1	108.6	164.3	189.8	178.7	79.8	244.8	158.7	75.2	116.3	143.1
CD <sub><i>t</i></sub> <sup>2</sup>	CD	8.6	11.3	13.5	14.7	14.9	14.0	23.8	20.5	6.3	<b>13.46</b>	14.6	10.4	13.1	13.8
	EMD	<b>33.8</b>	<b>32.5</b>	31.1	<b>29.2</b>	40.3	34.4	<b>82.0</b>	38.3	50.9	30.2	41.4	27.7	<b>38.4</b>	39.3
CD <sub><i>p</i></sub> <sup>2</sup>	CD	8.4	10.9	13.46	<b>14.5</b>	14.6	13.8	22.7	20.2	<b>6.0</b>	13.5	14.1	<b>10.3</b>	12.7	13.5
	EMD	41.0	33.2	<b>30.2</b>	31.0	<b>37.4</b>	<b>32.7</b>	83.7	<b>36.6</b>	<b>46.3</b>	<b>29.6</b>	<b>38.5</b>	<b>26.9</b>	38.5	<b>38.9</b>
OPTA	CD	4.3	6.7	11.6	11.1	9.2	9.5	5.0	13.6	2.3	10.6	8.9	9.2	5.4	8.3
	EMD	17.1	21.3	32.1	26.8	25.6	24.3	20.1	34.0	11.0	26.0	26.1	23.3	15.9	23.4
Tars3d	EMD	179.5	-	-	108.6	169.8	-	-	-	-	-	-	-	-	-

Table 4. The results of quantitative VC and IT on Atlasnet.  $N_{VC}$  and  $N_{VC'}$  are the average number of VC-related vertices, while  $F_{IT}$  and  $V_{IT}$  are the number of IT-related faces and vertices. Small results are preferred as well.

Method	Metric	airplane	bench	cabinet	car	chair	display	lamp	speaker	rifle	sofa	table	telephone	vessel	Avg.%
At <sub>CD</sub>	$N_{VC}$	188.9	167.7	30.5	30.2	80.9	43.6	257.2	38.9	367.2	35.8	130.6	35.5	142.6	4.7
	$N_{VC'}$	149.9	135.9	23.7	24.1	64.6	35.4	239.4	33.6	314.3	28.6	106.3	25.4	118.9	3.9
	$F_{IT}$	321.0	337.3	74.2	142.9	343.5	213.6	229.9	2.7	<b>486.7</b>	110.1	809.5	60.0	172.2	5.0
	$V_{IT}$	313.1	320.1	81.2	138.2	310.1	189.7	232.5	4.0	<b>450.5</b>	113.5	677.8	77.0	163.8	9.2
CD <sup>2</sup>	$N_{VC}$	357.1	329.5	72.9	44.7	117.5	162.5	242.9	57.9	383.9	115.0	235.5	121.9	166.8	7.2
	$N_{VC'}$	299.7	290.2	58.7	36.5	96.5	138.7	220.0	50.3	342.3	91.8	200.5	92.7	141.2	6.2
	$F_{IT}$	327.7	424.1	96.5	46.7	347.7	176.2	169.7	15.3	631.9	73.5	530.2	59.0	<b>55.5</b>	4.4
	$V_{IT}$	336.6	407.6	100.7	46.5	311.4	184.7	188.4	20.0	600.8	77.9	502.5	69.1	<b>69.7</b>	8.8
CD <sub><i>t</i></sub> <sup>2</sup>	$N_{VC}$	<b>182.3</b>	<b>156.5</b>	<b>20.1</b>	<b>7.9</b>	<b>67.4</b>	<b>42.5</b>	<b>120.1</b>	<b>21.1</b>	<b>213.1</b>	<b>27.4</b>	<b>114.6</b>	<b>29.1</b>	83.1	<b>3.3</b>
	$N_{VC'}$	<b>145.3</b>	<b>126.9</b>	<b>15.2</b>	<b>6.1</b>	<b>55.8</b>	<b>33.5</b>	<b>102.6</b>	<b>17.6</b>	<b>178.9</b>	<b>20.8</b>	<b>92.5</b>	<b>20.8</b>	66.8	<b>2.6</b>
	$F_{IT}$	<b>233.1</b>	<b>265.6</b>	<b>61.9</b>	<b>12.7</b>	<b>189.5</b>	<b>137.3</b>	<b>167.2</b>	<b>2.6</b>	<b>759.7</b>	<b>70.3</b>	<b>462.4</b>	<b>46.4</b>	152.2	<b>3.8</b>
	$V_{IT}$	<b>250.7</b>	<b>249.8</b>	<b>63.2</b>	<b>13.9</b>	<b>184.7</b>	<b>137.9</b>	<b>179.2</b>	<b>4.1</b>	<b>680.2</b>	<b>75.8</b>	<b>444.2</b>	<b>54.2</b>	148.2	<b>7.5</b>
CD <sub><i>p</i></sub> <sup>2</sup>	$N_{VC}$	223.2	193.3	28.9	22.6	90.7	54.8	147.5	30.9	233.1	31.8	123.8	37.1	<b>72.8</b>	3.9
	$N_{VC'}$	181.2	158.5	22.4	17.4	75.1	42.2	129.5	25.1	194.6	25.9	101.1	28.9	<b>58.1</b>	3.2
	$F_{IT}$	285.8	300.2	86.4	26.4	293.0	233.5	187.9	<b>2.1</b>	601.6	<b>59.3</b>	529.5	59.0	96.9	4.1
	$V_{IT}$	299.8	296.9	86.3	32.2	283.2	209.5	195.7	<b>3.6</b>	537.4	<b>63.6</b>	474.9	60.8	97.4	7.9

echoed by the recent study [39]. Surprisingly, our CD<sub>*p*</sub><sup>2</sup> and CD<sub>*t*</sub><sup>2</sup> output some meshes whose EMD values closely approach to the OPTA value in Table 3. This indicates our results are almost optimal in terms of EMD metrics for the categories of cabinet, car, louder speaker, sofa, telephone, etc.

It should be mentioned that the classic scheme Atlasnet At<sub>CD</sub> only wins in CD value. This is because At<sub>CD</sub> use CD loss in the model training and thus CD values is almost minimized in At<sub>CD</sub>. Our methods were trained by CD<sup>2</sup> but measured with CD, which indicates that our proposals might have large CD values. However, this does not imply that At<sub>CD</sub> is better than our schemes. Both visual results and results of EMD metrics demonstrate that our proposed schemes outperform At<sub>CD</sub>. On the other hand, these results also demonstrate that CD might be appropriate for model training, while the metrics of EMD, our VC, IT, and the proposed DPVI are suitable for quality measurement.

## 4.2 Comparisons with 3DAF on ShapeNet

The latest CD-based scheme 3DAF [44], which has drastically improved the performance of the 3D reconstruction and completion task, utilizes 3D information contained in the CAD model of ShapeNet and the global 2D feature as semantic attributes flow. We implement our proposal CD<sup>2</sup> in 3DAF and calculate the average value of all the categories. Both CD and EMD metrics are computed by the official codes provided in 3DAF [44]. For the VC problems, the metrics of  $N_{VC}$  and  $N_{VC'}$  are calculated similarly to Section 4.1. Since 3DAF is proposed for point cloud reconstruction tasks, there does not exist face information in the output. We use the API *create\_from\_point\_cloud\_alpha\_shape* [51] in open3d [46] to iteratively generate a mesh with the maximum face number  $F_{\alpha}$ . We denote the number of vertices in this mesh by  $V'_{IT}$ . We employ another API *create\_from\_point\_cloud\_ball\_pivoting* [47, 48] in open3d to generate a mesh with the maximum face number  $F_{bpa}$  and then obtain the IT-related face number as  $F'_{IT} = (F_{bpa} + F_{\alpha})/2$ . In short, IT problems are quantified by  $V'_{IT}$  and  $F'_{IT}$  in this subsection. As a baseline, 3DAF is provided by the author in [44]. Our CD<sup>2</sup>s in 3DAF are trained with 100 epochs. Some experimental settings are listed as follows:  $p_d = 0.3$  and  $d_T = 10^{-7}$  for CD<sup>2</sup>;  $pvi_t = 4$  for CD<sub>t</sub><sup>2</sup>; and  $pvi_p = 0.08$  for CD<sub>p</sub><sup>2</sup>. Other settings are identical with 3DAF in [44].

Table 5. Results with 3DAF. CD is multiplied by 1000, and EMD is multiplied by 100.

Methods/Metrics	CD	EMD	$N_{VC}$	$N_{VC'}$	$V'_{IT}$	$F'_{IT}$
3DAF	<b>4.06</b>	5.56	141.9	71.9	1662.9	2951
CD <sup>2</sup>	4.71	5.99	338.2	181	1606.3	2777.3
CD <sub>t</sub> <sup>2</sup>	7.1	5.7	362.2	160.9	<b>1915.1</b>	<b>3565.6</b>
CD <sub>p</sub> <sup>2</sup>	6.06	<b>5.49</b>	<b>105.5</b>	<b>48.4</b>	1898	3532.4

We present our results in Table 5. We can easily find that our CD<sub>t</sub><sup>2</sup> and CD<sub>p</sub><sup>2</sup> dominate 3DAF in terms of all the metrics except CD value. Our CD<sub>p</sub><sup>2</sup> reduces VC-related vertices by 25.6% on average. Meanwhile, more faces will be generated by the API of open3d when the reconstruction scheme outputs well-structured point clouds. Compared with 3DAF, our scheme increase the number of faces by 19.7%. Finally, 3DAF only wins for the metric of CD mainly because CD is used as the loss function during the training.

## 4.3 Comparisons with Total3D on Pix3D

Another recent work Total3D [21] studies 3D indoor reconstruction and scene understanding task and achieves smaller CD value on Pix3D dataset than other famous results [7, 12]. Pix3D is a large-scale dataset of well-aligned 2D images and 3D shapes. It consists of 10,069 image-shape pairs from 395 different indoor furniture in 9 categories. In this paper, we compare with two Total3D models, i.e., a pretrained model T3D<sub>pre</sub> provided by Total3D [21], a T3D<sub>CD</sub> model trained from scratch with codes offered in Total3D. We also implement our CD<sup>2</sup> and CD<sub>t</sub><sup>2</sup> in Total3D and train them from scratch without any pretrained models. In our CD<sup>2</sup>, we set  $p_{del} = 0.6$ ,  $d_T = 0$ , and learning rate is  $10^{-4}$ . In CD<sub>t</sub><sup>2</sup>,  $pvi_t = 4$ , and learning rate is  $10^{-5}$ . The train-test split is similar to [11] for all the models, and we use the object label mapping in NYU-37 [30].

We first present the visual comparisons of seven classes from different views in Fig. 6. These results are generated by T3D<sub>pre</sub>, T3D<sub>CD</sub>, and CD<sup>2</sup>. We render these meshes with the tool of Meshlab [8]. We can easily find that meshes produced by T3D<sub>pre</sub> and T3D<sub>CD</sub> have severe IT and VC problems in Fig. 6. For example, beds have an obvious fold on the left side; chairs have some



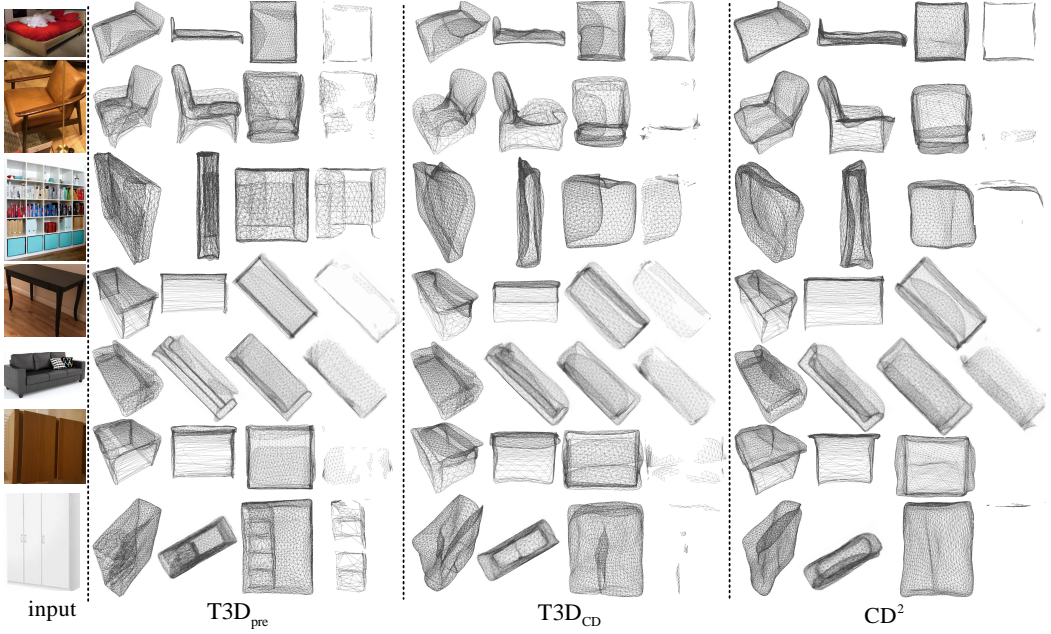


Fig. 6. Meshes on Total3D. We present the results for three methods T3D<sub>pre</sub>, T3D<sub>CD</sub>, and CD<sup>2</sup>. For each method, we show the output mesh from three different perspectives and its invisible faces in columns from left to right.

faces folded in cushions; and both bookcase and tables have twists inside the shelf and desktop. Fortunately, our CD<sup>2</sup> produces meshes with much fewer twists in most classes. For instance, the mesh structure of beds generated by our CD<sup>2</sup> is also more reasonable than T3D<sub>pre</sub>. Although meshes of sofa and table are not perfect in CD<sup>2</sup>, they are still better than these two baselines.

Another interesting result relates to invisible faces in mesh, shown in the last columns of each method in Fig. 6. We delete all the visible faces with tools of “select Faces in a rectangular region” and “select only visible” functions in MeshLab [8]. From the results of T3D<sub>pre</sub> and T3D<sub>CD</sub>, we find that there are large quantities of invisible faces in the interior mesh, and most of them have IT problems. This problem becomes even worse for the categories of bed, chair, bookcase, and table. On the contrary, our scheme CD<sup>2</sup> has few invisible faces. We even have no invisible faces for table. These findings demonstrate our scheme generates more faces to model the surface of objects and outputs well-structured meshes.

We also perform quantitative comparisons among three models, i.e., the official T3D<sub>pre</sub>, our CD<sup>2</sup>, and CD<sub>t</sub><sup>2</sup>. The results of IT and VC problems on Total3D dataset are shown in Table 6. Our experiment results demonstrates the proposed CD<sub>t</sub><sup>2</sup> outperforms T3D<sub>pre</sub> again, especially for IT problems. In detail, the output mesh in T3D<sub>pre</sub> has more than 28.10% faces and 46.44% vertices of IT problems. However, the IT-related faces of our CD<sub>t</sub><sup>2</sup> are only half of T3D<sub>pre</sub>. In addition, our CD<sub>t</sub><sup>2</sup> is better than CD<sup>2</sup>, which is consistent with the previous results on Atlasnet in Section 4.1. Finally, CD<sub>t</sub><sup>2</sup> have more VC vertices for four categories, i.e., chair, desk, table, and wardrobe, compared with T3D<sub>pre</sub>. This is because we move some invisible vertices to the surface of object, which efficiently reduces the IT problem and shortens the vertex distance. But this phenomenon only exists in a few special categories, and our schemes alleviate VC and IT simultaneously for most categories.

Table 6. The quantitative results of VC and IT on Total3D. All the columns except the last one represent the average quantity in terms of different metrics for each category, while the last one is the average percentage across all the categories. The smaller is better. Each sample consists of 2,562 vertices and 5,120 faces.

Method	Metric	bed	bookcase	chair	desk	msic	sofa	table	tools	wardrobe	Avg.%
T3D <sub>pre</sub>	Nvc	263.3	523.7	<b>489.5</b>	<b>644.8</b>	440.5	180.3	<b>347.9</b>	461.5	<b>190.9</b>	15.36
	Nvc'	200.0	446.5	<b>423.2</b>	<b>559.8</b>	381.8	129.4	<b>285.0</b>	403.7	<b>149.2</b>	12.92
	Fit	893.1	1265.5	1549.5	2283.0	1334.4	777.6	1429.5	2834.2	581.9	28.10
	Vit	830.1	1174.7	1281.9	1763.6	1133.5	729.8	1211.9	2054.7	528.9	46.44
CD <sup>2</sup>	Nvc	464.8	892.4	923.0	1051.6	574.9	228.8	731.6	500.8	322.8	24.68
	Nvc'	389.2	816.2	832.1	974.8	520.9	174.5	630.6	431.5	259.7	21.81
	Fit	909.6	1195.7	1479.4	1777.6	682.5	838.0	1238.4	1858.6	511.8	22.77
	Vit	860.4	1001.3	1243.9	1484.5	648.2	809.0	1053.6	1445.2	497.9	39.22
CD <sub>t</sub> <sup>2</sup>	Nvc	<b>148.0</b>	<b>456.5</b>	590.5	671.7	<b>175.5</b>	<b>74.7</b>	526.4	<b>151.8</b>	287.8	<b>13.37</b>
	Nvc'	<b>121.2</b>	<b>419.1</b>	521.8	610.8	<b>152.4</b>	<b>58.1</b>	459.3	<b>124.7</b>	243.5	<b>11.76</b>
	Fit	<b>344.4</b>	<b>642.2</b>	<b>941.9</b>	<b>1351.2</b>	<b>351.5</b>	<b>275.8</b>	<b>725.9</b>	<b>1002.0</b>	<b>392.7</b>	<b>13.08</b>
	Vit	<b>356.4</b>	<b>560.9</b>	<b>867.6</b>	<b>1171.4</b>	<b>352.3</b>	<b>285.7</b>	<b>678.7</b>	<b>946.4</b>	<b>381.3</b>	<b>24.29</b>

We show the EMD results on Total3D for T3d<sub>pre</sub>, our CD<sup>2</sup>, and CD<sub>t</sub><sup>2</sup> in Table 7. Our schemes achieve smaller EMD results than the CD-based T3d<sub>pre</sub> on average. For the classes of bed, chair, desk, and table, the Total3D baseline T3d<sub>pre</sub> performs slightly better than our schemes. The reasons are similar to the results of VC explained above. In other words, the IT-related vertices may reduce the VC value and the EMD metric since fewer vertices are located at the surface of meshes.

Table 7. EMD results on Total3D. All the presented results have been divided by 100, and the last column shows the average value for each method. The smaller is better.

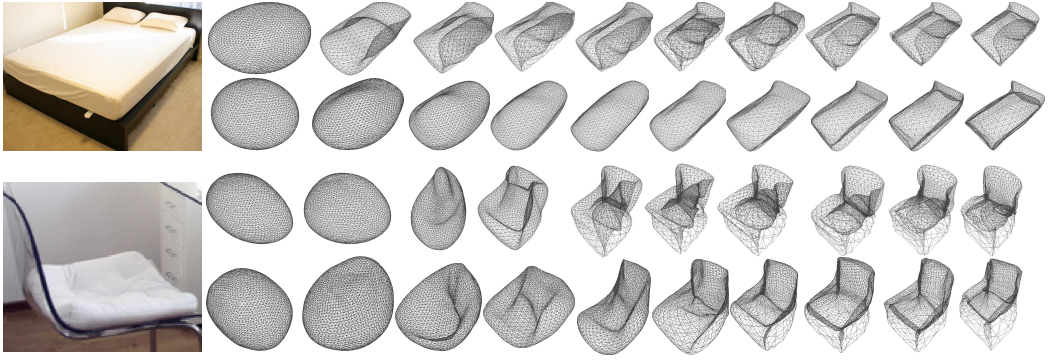
	bed	bookcase	chair	desk	msic	sofa	table	tools	wardrobe	Avg
T3D <sub>pre</sub>	<b>2.71</b>	12.88	<b>4.81</b>	<b>5.98</b>	11.69	2.14	<b>6.52</b>	13.67	7.42	7.54
CD <sup>2</sup>	3.64	11.72	8.00	7.94	10.84	<b>1.88</b>	6.55	<b>8.33</b>	<b>2.89</b>	6.87
CD <sub>t</sub> <sup>2</sup>	3.85	<b>9.99</b>	6.07	6.42	<b>10.30</b>	2.24	6.89	8.95	4.86	<b>6.62</b>
Im3d	1.83	0.91	1.74	2.01	2.82	0.82	2.71	0.67	0.74	1.58

We also confirm some observations from visual comparisons with quantitative results. We randomly select ten samples from some categories and calculate the average number of invisible faces and show the results in Table 8. From our results, we ensure that a mesh produced by CD<sup>2</sup> has fewer invisible faces than T3D<sub>CD</sub> and T3D<sub>pre</sub> for almost all the categories. These results show that more faces contribute to the surface of objects, which benefits the generation of well-structured mesh.

In this subsection, we also demonstrate the deformation process of two samples in Fig. 7. In the 1st and 3rd rows, we can find the generation process of folds and twists caused by the CD on Total3D dataset. However, our CD<sup>2</sup> shown in the 2nd and 4th rows succeeds in approaching the target object by performing the fine-grained orchestration of vertex deformation, instead of the brute-force nearest neighbour search and minimal gradient procedure, and implementing an

Table 8. The quantity of invisible faces for generated meshes. Smaller values are preferred.

Method	Bed	Bookcase	Chair	Desk&Table	Sofa
T3D <sub>pre</sub>	604	890.6	473.8	377.8	<b>1071.7</b>
T3D <sub>CD</sub>	979	1023.4	499.2	428.4	1307.7
CD <sup>2</sup>	<b>310</b>	<b>386.8</b>	<b>139</b>	<b>17.2</b>	1081

Fig. 7. Meshes deformation during learning progress. Meshes are generated by T3D<sub>CD</sub> for the 1st and 3rd row, while other results are obtained from CD<sup>2</sup>.

adaptive and effective deformation without obvious folds and twists. Fig. 7 is a significant proof of performance improvement with our CD<sup>2</sup>.

#### 4.4 Comparisons with SDF-based schemes

Recently, some implicit 3D representation methods like SDF-based schemes are becoming popular and attracting much attention in academia. In this paper, we also compare our work with two state-of-the-art implicit representation methods Im3d [45] and Tars3d [50]. We evaluate these schemes with the EMD metric and show the results. In Table 3, compared with At<sub>CD</sub>, Tars3d achieves larger EMD values for all three categories it trained on. Meanwhile, our CD<sub>t</sub><sup>2</sup> has much smaller EMD values than Tars3d. It should be noted that our CD<sub>t</sub><sup>2</sup> is trained on all 13 categories, while Tars3d is trained separately for each category. In addition, we find that Tars3d cannot model objects accurately for some specific parts in Fig. 8. For instance, meshes of airplane cabin and chair backrest are not properly reconstructed, they tend to be smaller than the target object. However, Im3d performs better than Total3D and our CD<sup>2</sup>s in terms of EMD metrics, as shown in Table 7. The performance improvement of Im3d can also be found in Fig. 8.

We also show the DPVI results of these two SDF-based schemes in Table 2, and find that they both perform worse than our CD<sub>t</sub><sup>2</sup> and CD<sub>p</sub><sup>2</sup>. In practice, SDF-based schemes might introduce additional problems like some impending parts shown by the red circle in Fig. 8. Even worse, SDF-based schemes might generate chaotic and unusable meshes when the input image has dim light and cluttered background. We show this problem with a table mesh in Fig. 8. These two problems contribute to the increase of DPVI. In sum, our schemes outperform two SDF-based schemes in terms of DPVI and dominate Tars3d in terms of EMD.

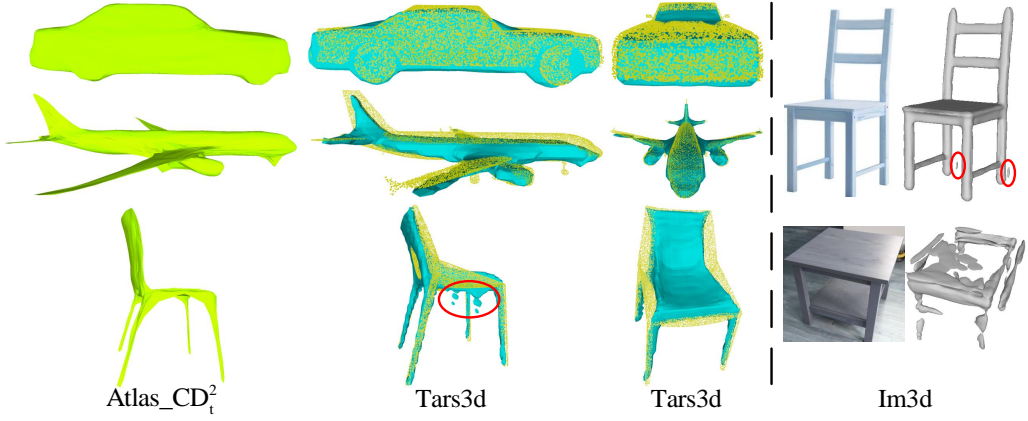


Fig. 8. Mesh reconstruction results of Atlas\_CD<sub>t</sub><sup>2</sup>, Tars3d, and Im3d. We use yellow dots to denote the ground truth 3D points and red circles to highlight the impending parts of meshes.

#### 4.5 Time consumption of CD, EMD, and CD<sup>2</sup>s

We show the time consumption of three metrics CD, EMD, and CD<sup>2</sup>s to calculate the distance between two point sets  $S_1$  and  $S_2$  for 1,000 times. The results are shown in Fig. 9. Except for the EMD metric, all the results increase linearly as the quantity of points increases. In addition, we can find that the time consumption of CD<sup>2</sup> is close to that of CD, but our CD<sub>p</sub><sup>2</sup> and CD<sub>t</sub><sup>2</sup> have larger slopes because mapping-related vertex elimination operation consumes more time than distance-based method. On the other hand, the EMD metric has an exponential rise in time consumption, which is much larger than CD-based metrics. When there are 10,000 points in the point set, the computation time is more than 1.20s for the each EMD calculation. Compared with EMD, our CD<sup>2</sup>s are more computation-efficient.

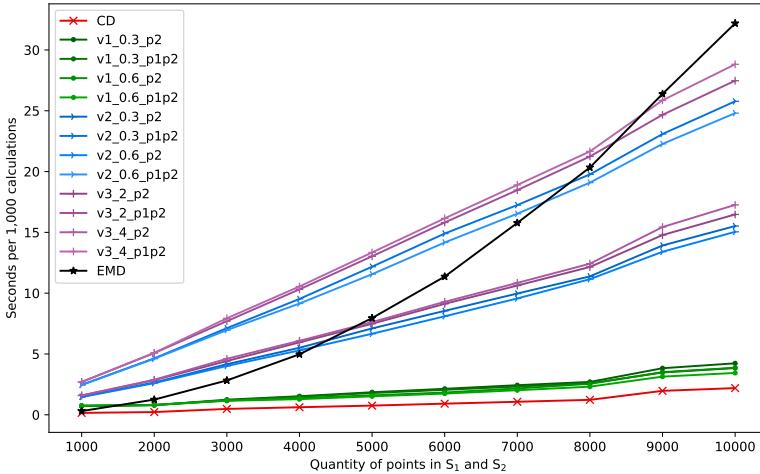


Fig. 9. The time consumption of CD, EMD, and CD<sup>2</sup>s. The EMD result is divided by 45. In the legend, v1, v2, and v3 are separately CD<sub>t</sub><sup>2</sup>, CD<sub>p</sub><sup>2</sup>, and CD<sub>t</sub><sup>2</sup>. The following decimals are the exclusion percentage ( $p_d$  and  $p_{vip}$ ), while the integers indicate the exclusion threshold ( $p_{vit}$ ). p2 means the only exclusion of  $S_2$ , and p1p2 means the exclusion of  $S_1$  and  $S_2$  simultaneously.

## 5 RELATED WORK

In this section, we review some representation methods and machine-learning-enabled techniques in 3D reconstruction. Then, some major metrics are surveyed for the loss function, and we mainly discuss the CD loss in the explicit mesh deformation process.

### 5.1 3D Reconstruction with Machine Learning

There exists a variety of studies in the field of 3D reconstruction from RGB images using promising machine learning techniques. In these studies, the output format of 3D objects includes point cloud [17, 23, 39], voxel [28, 36, 40], primitives [12], mesh [21], etc. Among them, mesh appeals to complicated topology and can represent any 3D object accurately and efficiently. For the 3D mesh reconstruction, one line of studies generates mesh by using SDF [9] and other implicit surfaces [22]. For instance, Zhang et al. learned a 3D shape as local implicit information and then decoded it to SDF values [45]. Duggal and Pathak mapped the input 3D point clouds to canonical space and then employed DeformNet and shape generator to generate SDF [50]. In this category of research, the marching cube algorithm [49] is adopted to obtain the final mesh from the intermediate SDF. Meanwhile, another line of impressive studies explicitly and directly reconstructs a mesh from a template with deformation methods, which are the focus of this paper. Early works can only produce a category-specific mesh by transforming a learned mean shape [32]. Recently, some studies have been presented to yield meshes by deforming different initial templates. For example, Pontes et al. obtained a compact mesh representation by deforming an initial cube shape [26]. Gkioxari et al. converted the coarse voxel to mesh by refining the vertices and edges with graph convolution network [11]. Wang et al. progressively deformed an ellipsoid to the target object by utilizing the perceptual features from images [37]. In [12], Groueix et al. even supported mesh deformation with different amounts of spheres or squares called primitives. Besides these results, Huang et al. applied multi-view renderings with a 3D human template to a deformation model and achieved photo-consistency human meshes [42]. Chen et al. folded a 2D lattice to the target object and then learned a pairwise mapping between the 3D data [7]. In [21], Nie et al. further explored the main differences and impacts between cutting edges and removing faces in the topology modification operations [24].

### 5.2 Metrics of 3D Reconstruction

CD [2], Earth Mover Distance (EMD) [27], and Intersection over Union (IoU) are widely-adopted metrics to measure the distance between reconstructed mesh and the target object point set in current researches. Since IoU is not differentiable, most works use CD and EMD as their loss functions in deep learning models as well as metrics to evaluate the quality of reconstructed mesh [6, 11, 12, 21, 37, 42]. CD calculates the nearest pair-wise distance from one point set to the other one, while EMD relies on solving an optimization problem to obtain the best mapping function from one set to the other set. Although EMD is more faithful than CD, the computation cost of CD (i.e.,  $O(N \times \log(N))$ ) is much smaller than that of EMD (i.e.,  $O(N^3 \times \log(N))$ ) [29]. In addition, CD can be calculated in parallel and further accelerated by KD-tree [3] and Octree [18]. Besides the above metrics, DPDist [33] and the sliced Wasserstein distance [4] are also proposed in recent years, but they are not the mainstream metrics in various tasks. In this paper, we concentrate on the preferable CD and improve it in the model training and evaluation.

### 5.3 Chamfer Distance

Some severe problems have been identified for the CD loss in deep learning model. For instance, Achlioptas et al. discovered that CD is prone to generate outputs with points crowded in the area

with highest occupancy probability (e.g. the seat of chairs), and there exists the imbalance problem between two summands  $CD_{S_1}$  and  $CD_{S_2}$  [1]. Li et al. showed that CD suffers from the local optimum problem in the nearest neighbor search of a finger moving example [14]. In [13], Jin et al. found that thickening, elongating, and shortening four legs of a chair result in a larger CD value than removing any leg, which implies that CD is not faithful visually and structurally. By comparing the loss of CD with Mean Squared Error (MSE) in model training, Wagner et al. discovered that optimizing CD directly would neglect some details especially for densely-sampled point cloud [34]. In [25], Paschalidou et al. pointed out that Atlasnet with optimized CD would generate zero-volume primitives and faces with inverted normal. Their observations partially and implicitly demonstrate the self-intersection problem induced by CD. In a nutshell, the IT and VC problems caused by CD loss have not been explicitly discovered before in the deformation process, which is one of the contributions in this paper.

Meanwhile, some variant CDs have been proposed to improve the deformation performance. Li et al. proposed a structured CD scheme which divides 3D objects into several regions and computes the nearest neighbour search in a region-to-region manner other than an all-to-all manner [14]. Lim et al. provided a sharper version of CD, which summarizes the  $p$  power of each distance over all the points and then computes its  $p$ -th root [16]. Their scheme punishes points with large errors more heavily than before. In [35], Wang et al. proposed an adaptive CD loss for better aligning partial shapes. In detail, they obtained the overlapping subset for each point set with a pre-defined distance threshold and then applied CD to these two overlapping subsets. In the optimization process, the pre-defined distance threshold is chosen adaptively. Li et al. presented a probabilistic CD loss for accurate key point localization in [15]. Chen et al. proposed an augmented CD by only choosing the largest term each time [7]. The most relevant work is [39], where Wu et al. proposed a Density-aware CD (DCD) for balanced point cloud reconstruction. DCD considers each vertex equally in terms of its queried frequency and then lessens the impact of outliers. In comparison, our work concentrates on mesh reconstruction and treats vertices of mesh unequally with moderate speeds and correct directions. In this way, we endeavor to orchestrate the deformation process to mitigate the IT and VC problems, which is another contribution of this paper.

Some additional constraints are added to the CD loss function to improve local details of mesh. These auxiliary constraints include factual constraints and hypothetical assumptions. For the first category, the edge distance constraint avoids merging adjacent edges [11]; Laplacian loss [10] and normal loss [37] both impose the smoothness of mesh; boundary regularization enforces smoothness and consistency of boundary curves [24]; and locality loss penalizes points which locates outside of a small spatial region [16]. For the second group of auxiliary constraints, unup3d in [38] assumed that all human faces were symmetric and added this assumption to the loss function. Alex et al. studied how the physics-inspired prior knowledge impacts the model to learn dynamics, hypothesizing that all real-world video datasets obey the law of physics [5]. Michael et al. even argued that deep-learning-enabled methods cannot survive without prior knowledge [22]. Finally, it should be noted that these auxiliary constraints are orthogonal to our paper.

## 6 CONCLUSION

In this paper, we have identified that CD loss may introduce VC and IT problems in explicit mesh reconstruction and then provided fine-grained deformation schemes  $CD^2$ s to orchestrate the deformation of vertices and alleviate these two problems. Our schemes first compute CD loss to exclude aggressively-deformed vertices with distance or mapping information and then move a subset of vertices to the ground truth points with a second CD calculation. We have implemented our  $CD^2$ s in three representative CD-based schemes, Atlasnet, 3DAF, and Total3D, on two datasets, ShapeNet and Pix3D. We compare our  $CD^2$ s with these baselines in terms of various metrics, most

of which are newly proposed by our paper. Extensive experimental results show that our proposals outperform the baselines for most of the categories and produce more plausible and well-structured meshes. We also compare two implicit SDF-based reconstruction schemes with our proposals and find that our CD<sup>2</sup>s dominate SDF-based schemes in terms of DPVI metric. Results show that these two lines of mesh reconstruction mechanisms have their own advantages and benefits. Some theoretical studies of VC and IT problems will benefit 3D mesh reconstruction, and we leave them in future work.

## REFERENCES

- [1] ACHLIOPTAS, P., DIAMANTI, O., MITLIAGKAS, I., AND GUIBAS, L. Learning representations and generative models for 3d point clouds. In *International conference on machine learning* (2018), PMLR, pp. 40–49.
- [2] BARROW, H. G., TENENBAUM, J. M., BOLLES, R. C., AND WOLF, H. C. Parametric correspondence and chamfer matching: Two new techniques for image matching. Tech. rep., SRI INTERNATIONAL MENLO PARK CA ARTIFICIAL INTELLIGENCE CENTER, 1977.
- [3] BENTLEY, J. L. Multidimensional binary search trees used for associative searching. *Communications of the ACM* 18, 9 (Sept. 1975), 509–517.
- [4] BONNEEL, N., RABIN, J., PEYRÉ, G., AND PFISTER, H. Sliced and radon wasserstein barycenters of measures. *Journal of Mathematical Imaging and Vision* 51, 1 (2015), 22–45.
- [5] BOTEV, A., JAEGLER, A., WIRNSBERGER, P., HENNES, D., AND HIGGINS, I. Which priors matter? benchmarking models for learning latent dynamics. *arXiv preprint arXiv:2111.05458* (2021).
- [6] CHANG, A. X., FUNKHOUSER, T., GUIBAS, L., HANRAHAN, P., HUANG, Q., LI, Z., SAVARESE, S., SAVVA, M., SONG, S., SU, H., ET AL. Shapenet: An information-rich 3d model repository. *arXiv preprint arXiv:1512.03012* (2015).
- [7] CHEN, S., DUAN, C., YANG, Y., LI, D., FENG, C., AND TIAN, D. Deep Unsupervised Learning of 3D Point Clouds via Graph Topology Inference and Filtering. *IEEE Transactions on Image Processing* 29 (2020), 3183–3198.
- [8] CIGNONI, P., CALLIERI, M., CORSINI, M., DELLEPIANE, M., GANOVELLI, F., RANZUGLIA, G., ET AL. Meshlab: an open-source mesh processing tool. In *Eurographics Italian chapter conference* (2008), vol. 2008, Salerno, Italy, pp. 129–136.
- [9] DAI, A., QI, C. R., AND NIEBNER, M. Shape Completion Using 3D-Encoder-Predictor CNNs and Shape Synthesis. In *2017 IEEE Conference on Computer Vision and Pattern Recognition (CVPR)* (Honolulu, HI, July 2017), IEEE, pp. 6545–6554.
- [10] DESBRUN, M., MEYER, M., SCHRÖDER, P., AND BARR, A. H. Implicit fairing of irregular meshes using diffusion and curvature flow. In *Proceedings of the 26th annual conference on Computer graphics and interactive techniques - SIGGRAPH '99* (Not Known, 1999), ACM Press, pp. 317–324.
- [11] GKIOXARI, G., JOHNSON, J., AND MALIK, J. Mesh R-CNN. In *2019 IEEE/CVF International Conference on Computer Vision (ICCV)* (Seoul, Korea (South), Oct. 2019), IEEE, pp. 9784–9794.
- [12] GROUEIX, T., FISHER, M., KIM, V. G., RUSSELL, B. C., AND AUBRY, M. A Papier-Mache Approach to Learning 3D Surface Generation. In *2018 IEEE/CVF Conference on Computer Vision and Pattern Recognition* (Salt Lake City, UT, USA, June 2018), IEEE, pp. 216–224.
- [13] JIN, J., PATIL, A. G., XIONG, Z., AND ZHANG, H. Dr-kfs: A differentiable visual similarity metric for 3d shape reconstruction. In *European Conference on Computer Vision* (2020), Springer, pp. 295–311.
- [14] LI, C.-L., SIMON, T., SARAGIH, J., POZOS, B., AND SHEIKH, Y. LBS Autoencoder: Self-Supervised Fitting of Articulated Meshes to Point Clouds. In *2019 IEEE/CVF Conference on Computer Vision and Pattern Recognition (CVPR)* (Long Beach, CA, USA, June 2019), IEEE, pp. 11959–11968.
- [15] LI, J., AND LEE, G. H. USIP: Unsupervised Stable Interest Point Detection From 3D Point Clouds. In *2019 IEEE/CVF International Conference on Computer Vision (ICCV)* (Seoul, Korea (South), Oct. 2019), IEEE, pp. 361–370.
- [16] LIM, I., IBING, M., AND KOBELT, L. A Convolutional Decoder for Point Clouds using Adaptive Instance Normalization. *Computer Graphics Forum* 38, 5 (Aug. 2019), 99–108.
- [17] LIN, C.-H., KONG, C., AND LUCEY, S. Learning efficient point cloud generation for dense 3d object reconstruction. In *proceedings of the AAAI Conference on Artificial Intelligence* (2018), vol. 32.
- [18] MEAGHER, D. Octree encoding: A new technique for the representation, manipulation and display of arbitrary 3-d objects by computer.
- [19] MESCHEDER, L., OECHSLE, M., NIEMEYER, M., NOWOZIN, S., AND GEIGER, A. Occupancy Networks: Learning 3D Reconstruction in Function Space. In *2019 IEEE/CVF Conference on Computer Vision and Pattern Recognition (CVPR)* (Long Beach, CA, USA, June 2019), IEEE, pp. 4455–4465.
- [20] NGUYEN, D., CHOI, S., KIM, W., AND LEE, S. GraphX-Convolution for Point Cloud Deformation in 2D-to-3D Conversion. In *2019 IEEE/CVF International Conference on Computer Vision (ICCV)* (Seoul, Korea (South), Oct. 2019), IEEE, pp. 8627–8636.



- [21] NIE, Y., HAN, X., GUO, S., ZHENG, Y., CHANG, J., AND ZHANG, J. J. Total3DUnderstanding: Joint Layout, Object Pose and Mesh Reconstruction for Indoor Scenes From a Single Image. In *2020 IEEE/CVF Conference on Computer Vision and Pattern Recognition (CVPR)* (Seattle, WA, USA, June 2020), IEEE, pp. 52–61.
- [22] OECHSLE, M., PENG, S., AND GEIGER, A. UNISURF: Unifying Neural Implicit Surfaces and Radiance Fields for Multi-View Reconstruction. In *2021 IEEE/CVF International Conference on Computer Vision (ICCV)* (Montreal, QC, Canada, Oct. 2021), IEEE, pp. 5569–5579.
- [23] PALA, P., AND BERRETTI, S. Reconstructing 3D Face Models by Incremental Aggregation and Refinement of Depth Frames. *ACM Transactions on Multimedia Computing, Communications, and Applications* 15, 1 (Feb. 2019), 1–24.
- [24] PAN, J., HAN, X., CHEN, W., TANG, J., AND JIA, K. Deep Mesh Reconstruction From Single RGB Images via Topology Modification Networks. In *2019 IEEE/CVF International Conference on Computer Vision (ICCV)* (Seoul, Korea (South), Oct. 2019), IEEE, pp. 9963–9972.
- [25] PASCHALIDOU, D., KATHAROPOULOS, A., GEIGER, A., AND FIDLER, S. Neural Parts: Learning Expressive 3D Shape Abstractions with Invertible Neural Networks. In *2021 IEEE/CVF Conference on Computer Vision and Pattern Recognition (CVPR)* (Nashville, TN, USA, June 2021), IEEE, pp. 3203–3214.
- [26] PONTES, J. K., KONG, C., SRIDHARAN, S., LUCEY, S., ERIKSSON, A., AND FOOKES, C. Image2mesh: A learning framework for single image 3d reconstruction. In *Asian Conference on Computer Vision* (2018), Springer, pp. 365–381.
- [27] RUBNER, Y., TOMASI, C., AND GUIBAS, L. J. The earth mover’s distance as a metric for image retrieval. *International journal of computer vision* 40, 2 (2000), 99–121.
- [28] SHIN, D., REN, Z., SUDDERTH, E., AND FOWLKES, C. 3D Scene Reconstruction With Multi-Layer Depth and Epipolar Transformers. In *2019 IEEE/CVF International Conference on Computer Vision (ICCV)* (Seoul, Korea (South), Oct. 2019), IEEE, pp. 2172–2182.
- [29] SHIRDHONKAR, S., AND JACOBS, D. W. Approximate earth mover’s distance in linear time. In *2008 IEEE Conference on Computer Vision and Pattern Recognition* (2008), IEEE, pp. 1–8.
- [30] SILBERMAN, N., HOIEM, D., KOHLI, P., AND FERGUS, R. Indoor segmentation and support inference from rgbd images. In *European conference on computer vision* (2012), Springer, pp. 746–760.
- [31] SUN, X., WU, J., ZHANG, X., ZHANG, Z., ZHANG, C., XUE, T., TENENBAUM, J. B., AND FREEMAN, W. T. Pix3D: Dataset and Methods for Single-Image 3D Shape Modeling. In *2018 IEEE/CVF Conference on Computer Vision and Pattern Recognition* (Salt Lake City, UT, USA, June 2018), IEEE, pp. 2974–2983.
- [32] TULSIANI, S., KAR, A., CARREIRA, J., AND MALIK, J. Learning Category-Specific Deformable 3D Models for Object Reconstruction. *IEEE Transactions on Pattern Analysis and Machine Intelligence* 39, 4 (Apr. 2017), 719–731.
- [33] URBACH, D., BEN-SHABAT, Y., AND LINDENBAUM, M. Dpdist: Comparing point clouds using deep point cloud distance. In *European Conference on Computer Vision* (2020), Springer, pp. 545–560.
- [34] WAGNER, N., AND SCHWANECKE, U. NeuralQAAD: An Efficient Differentiable Framework for Compressing High Resolution Consistent Point Clouds Datasets. In *Proceedings of the 17th International Joint Conference on Computer Vision, Imaging and Computer Graphics Theory and Applications* (Online Streaming, — Select a Country —, 2022), SCITEPRESS - Science and Technology Publications, pp. 811–822.
- [35] WANG, L., LI, X., AND FANG, Y. Deep-3daligner: Unsupervised 3d point set registration network with optimizable latent vector. *arXiv preprint arXiv:2010.00321* (2020).
- [36] WANG, M., WANG, L., AND FANG, Y. 3densinet: A robust neural network architecture towards 3d volumetric object prediction from 2d image. In *Proceedings of the 25th ACM international conference on Multimedia* (2017), pp. 961–969.
- [37] WANG, N., ZHANG, Y., LI, Z., FU, Y., LIU, W., AND JIANG, Y.-G. Pixel2mesh: Generating 3d mesh models from single rgb images. In *Proceedings of the European conference on computer vision (ECCV)* (2018), pp. 52–67.
- [38] WU, S., RUPPRECHT, C., AND VEDALDI, A. Unsupervised Learning of Probably Symmetric Deformable 3D Objects from Images in the Wild (Extended Abstract). In *Proceedings of the Thirtieth International Joint Conference on Artificial Intelligence* (Montreal, Canada, Aug. 2021), International Joint Conferences on Artificial Intelligence Organization, pp. 4854–4858.
- [39] WU, T., PAN, L., ZHANG, J., WANG, T., LIU, Z., AND LIN, D. Density-aware chamfer distance as a comprehensive metric for point cloud completion. *arXiv preprint arXiv:2111.12702* (2021).
- [40] XIE, H., YAO, H., SUN, X., ZHOU, S., AND ZHANG, S. Pix2Vox: Context-Aware 3D Reconstruction From Single and Multi-View Images. In *2019 IEEE/CVF International Conference on Computer Vision (ICCV)* (Seoul, Korea (South), Oct. 2019), IEEE, pp. 2690–2698.
- [41] YI-SHENG, Z., GUO-FU, D., YONG, H., AND XU, M.-H. Fast intersection algorithm between spatial triangles [j]. *Application Research of Computers* 10 (2008), 2906–2910.
- [42] YU, H., CHEANG, C., FU, Y., AND XUE, X. Multi-view Shape Generation for 3D Human-like Body. *ACM Transactions on Multimedia Computing, Communications, and Applications* (Feb. 2022), 3514248.
- [43] R. Zeng, C. Zeng, X. Wang, B. Li, and X. Chu, “Incentive mechanisms in federated learning and game-theoretical approach,” *IEEE Network*, pp. 1–7, 2022.



- [44] X. Wen, J. Zhou, Y.-S. Liu, H. Su, Z. Dong, and Z. Han, “3d shape reconstruction from 2d images with disentangled attribute flow,” in *Proceedings of the IEEE/CVF Conference on Computer Vision and Pattern Recognition (CVPR)*, June 2022, pp. 3803–3813.
- [45] C. Zhang, Z. Cui, Y. Zhang, B. Zeng, M. Pollefeys, and S. Liu, “Holistic 3d scene understanding from a single image with implicit representation,” in *Proceedings of the IEEE/CVF Conference on Computer Vision and Pattern Recognition*, 2021, pp. 8833–8842.
- [46] Q.-Y. Zhou, J. Park, and V. Koltun, “Open3D: A modern library for 3D data processing,” *arXiv:1801.09847*, 2018.
- [47] J. Digne, “An analysis and implementation of a parallel ball pivoting algorithm,” *Image Processing On Line*, vol. 4, pp. 149–168, 2014.
- [48] F. Bernardini, J. Mittleman, H. Rushmeier, C. Silva, and G. Taubin, “The ball-pivoting algorithm for surface reconstruction,” *IEEE transactions on visualization and computer graphics*, vol. 5, no. 4, pp. 349–359, 1999.
- [49] W. E. Lorensen and H. E. Cline, “Marching cubes: A high resolution 3d surface construction algorithm,” *ACM siggraph computer graphics*, vol. 21, no. 4, pp. 163–169, 1987.
- [50] S. Duggal and D. Pathak, “Topologically-aware deformation fields for single-view 3d reconstruction,” in *Proceedings of the IEEE/CVF Conference on Computer Vision and Pattern Recognition*, 2022, pp. 1536–1546.
- [51] H. Edelsbrunner and E. P. Mücke, “Three-dimensional alpha shapes,” *ACM Transactions on Graphics (TOG)*, vol. 13, no. 1, pp. 43–72, 1994.